Supporting Information

π-Aromatic Bi_5^- – The Heaviest Analogue of Cyclopentadienide $(C_5H_5)^-$ Finally Captured in the Mixed-Valent Compound $[\{IMesCo\}_2(\mu,\eta^5{:}\eta^5\text{-}Bi_5)]$

Julia Reinmüller,[a] Benjamin Peerless,[a] Sagar Paul,[b] Wolfgang Wernsdorfer,[b,c] Florian Weigend,[d]* and Stefanie Dehnen[a]*

[a] Institute of Nanotechnology, Karlsruhe Institute of Technology, Kaiserstrasse 12, 76131 Karlsruhe, Germany.
[b] Physikalisches Institut, Karlsruhe Institute of Technology, Wolfgang-Gaede-Str. 1, 76131 Karlsruhe, Germany.
[c] Institute of Quantum Materials and Technology, Karlsruhe Institute of Technology, Kaiserstrasse 12, 76131 Karlsruhe, Germany.
[d] Fachbereich Chemie, Philipps-Universität Marburg, Hans-Meerwein-Strasse 4, 35032 Marburg, Germany.

Table of Content

1 Single-Crystal Diffraction and Refinement Data

1.1 Crystal Measurement and Refinement Details

The data sets were collected on a Bruker D8 Quest with microfocus source emitting MoK_α radiation (λ = 0.71073Å) and a Photon 100 detector at T = 100 K. The structures were solved by dual space methods of SHELXT-2018/2 within the Olex2-1.3 software and refined using least-squares procedures on a F_2 with SHELXL-2018/3 in Olex2.[1] General crystallographic data are listed in **Supplementary Table 1**.

Supplementary Table 1 | Crystal data and details of the structure determination of compound 1.

Compound	**1**
Empirical formula	C_{42} H_{48} Bi_5 Co_2 N_4
Chemical formula	[{IMesCo}$_2$(μ,η^5:η^5-Bi_5)]
Emp. formula weight [g mol^{-1}]	1771.60
Temperature [K]	100
Crystal color, shape	metallic dark black, block
Crystal system	orthorhombic
Space group (no)	*Pccn* (56)
a [Å]	17.1783(12)
b [Å]	15.058(3)
c [Å]	17.048(4)
V [Å^3]	4409.7(14)
Z	4
ρ_{calc} [g cm^{-3}]	2.668
μ [mm^{-1}]	20.646
F(000)	3188
Crystal size	0.35 × 0.05 × 0.1
Radiation	Mo Kα
2θ range [°]	4.318-66.258
Index ranges	$-26 \le h \le 26$, $-23 \le k \le 23$, $-25 \le l \le 0$
Absorption correction type	Multi-scan
Reflections collected	29599
Ind. reflections / *R*(int) / *R*(sigma)	8349 / 0.0392 / 0.0351
Restraints / parameters	0 / 246
Final *R* indexes [$I \ge 2\sigma(I)$]	R_1 = 0.0269, wR_2 = 0.0552
Final *R* indexes [all data]	R_1 = 0.0362, wR_2 = 0.0573
Goodness-of-fit on F^2	1.064
Max peak / hole [e Å^{-3}]	1.470 / –1.793
CCDC number	2362176

2 Light microscopic Images of the Single crystals

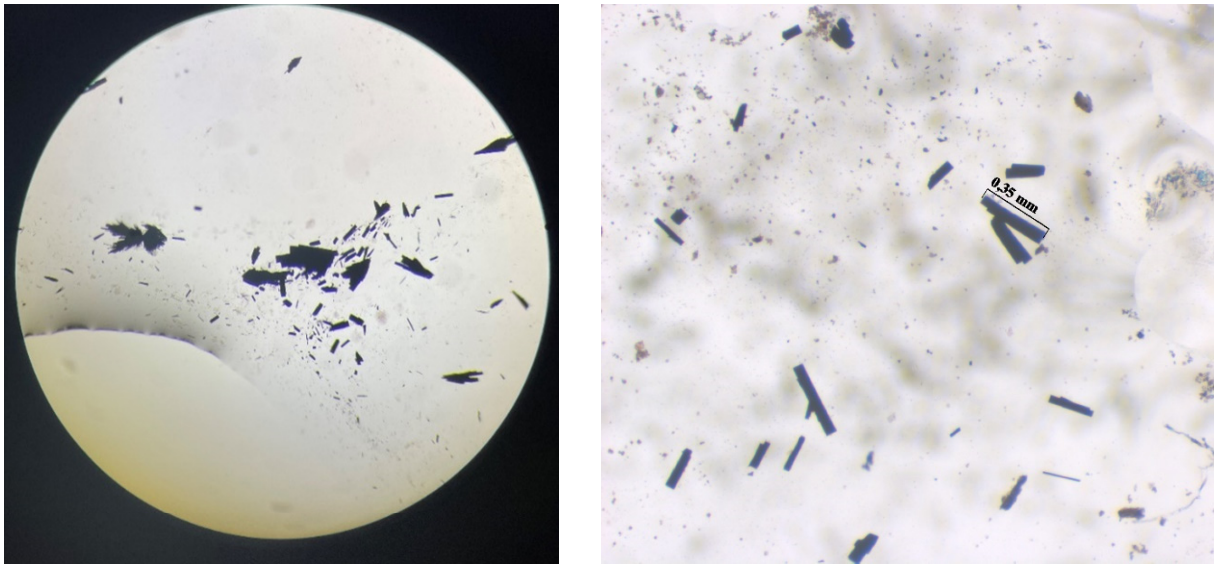

Supplementary Figure 1 | Crystal photographs of compound 1 taken through a light microscope. The scale bar in the figure on the right-hand side indicates the typical size of the single crystals.

3 Supplementary Structural Figures

All non-hydrogen atoms were refined using anisotropic displacement parameters. All hydrogen atoms were refined by using a riding model. Absorption correcting was carried out using MULTISCAN. Supplementary structural figures are shown in **Supplementary Figure 2** and **Supplementary Figure 3**. The structures were drawn with DIAMOND.[2] They are shown with displacement ellipsoids at the 50% probability level for non-hydrogen atoms.

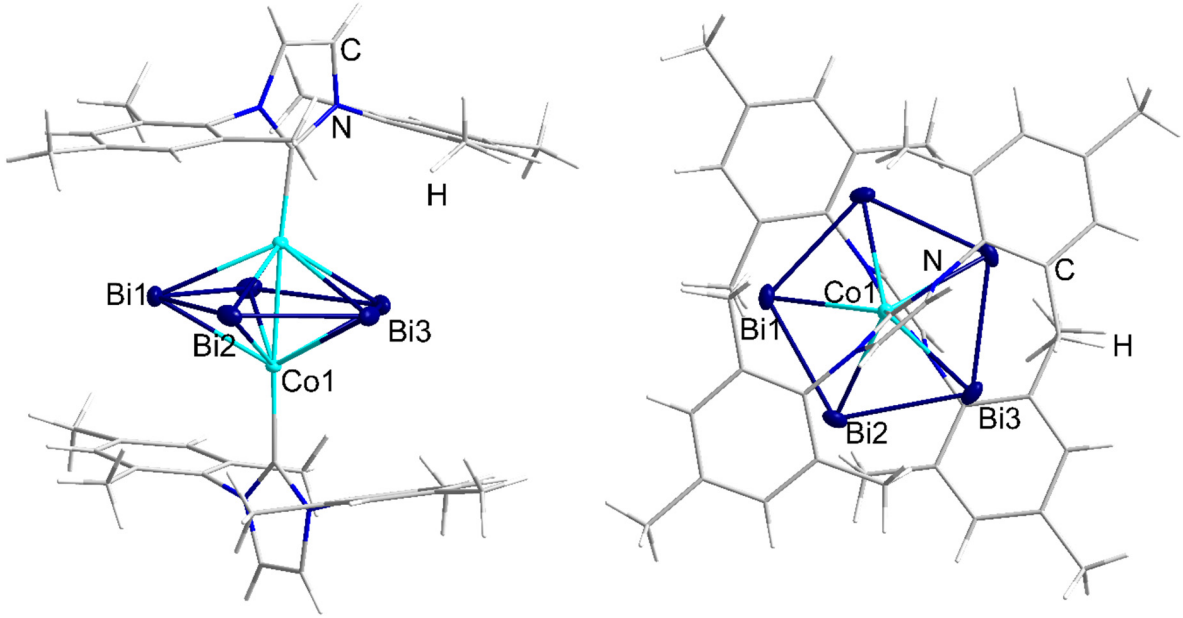

Supplementary Figure 2 | Two views of the molecular structure of compound 1 with all H atoms shown and atoms of the asymmetric unit labelled. Displacement ellipsoids are shown with 50% probability for non-H atoms; organic groups are given in wire mode. Color code: Bi, dark blue; Co, turquoise; C, grey, N, blue; H, white.

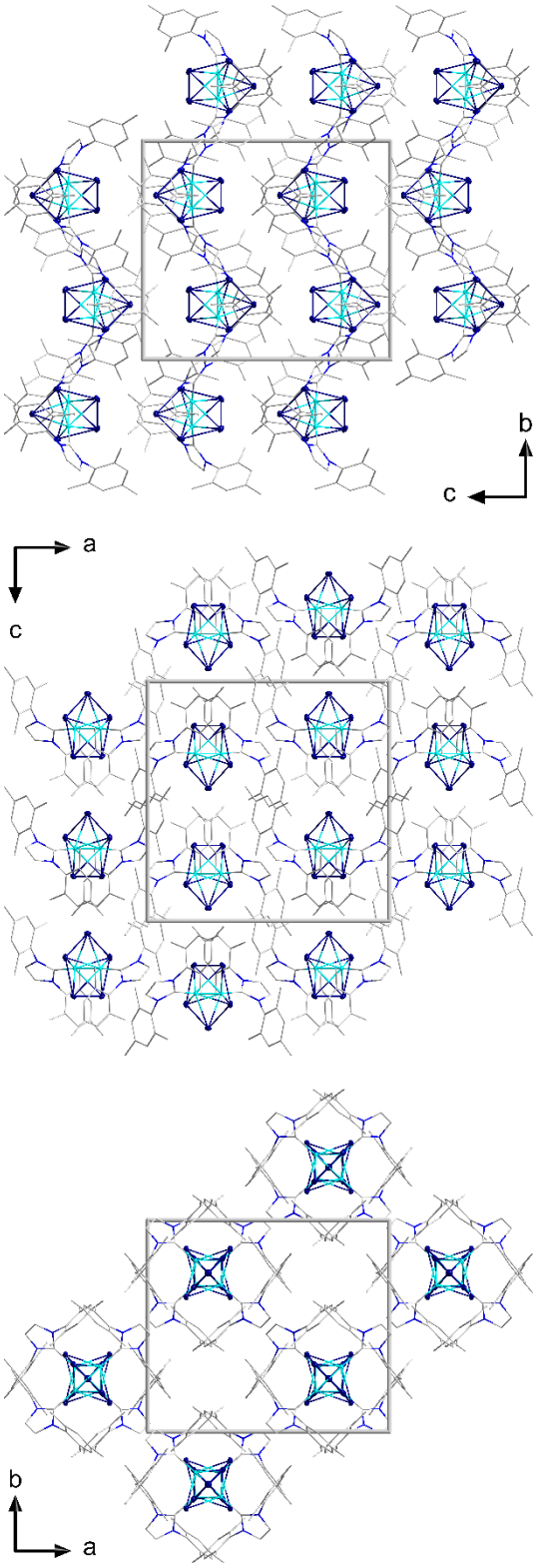

Supplementary Figure 3 | Views of the extended unit cell of compound 1 viewed along crystallographic axes *a*, *b*, and *c* (from top). Displacement ellipsoids are shown with 50% probability for non-H atoms; H atoms are not shown for clarity. Color code: Bi, dark blue; Co, turquoise; C, grey, N, blue.

4 Micro-X-Ray Fluorescence Spectroscopy (µ-XFS)

All µ-XFS measurements were performed on a Bruker M4 Tornado, equipped with an Rh-target X-ray tube and a silicon drift detector. Quantification of the elements is achieved through deconvolution of the spectra. The results are summarized in **Supplementary Table 2**. The rhodium content from the target is omitted from the quantification results. The spectrum for single crystals of compound **1** is shown in **Figure 2d** in the main document along with the results of the deconvolution algorithm.

Supplementary Table 2 | Summary of the micro-X-ray fluorescence spectroscopy results.

Element	Atomic Nr.	Mass[%]	Atom Cont. Obs. [%]	Atom cont. Calc. [%]
Bi	83	89.9	71.6	71.4
Co	27	10.1	28.4	28.6

5 Electrospray ionization mass spectrometry (ESI-MS) investigations of the reaction solutions during the formation of 1

5.1 Methods

All mass spectra were recorded with a Thermo Fischer Scientific Finnigan LTQ-FT spectrometer in negative ion mode, ESI(–). The solutions were injected into the spectrometer with gastight 250 µL Hamilton syringes by syringe pump infusion. All capillaries within the system were washed with dry *o*-DFB 2 hours before and at least 10 min in between parameters were used: Spray Voltage: 3.6 kV, Capillary Temp: 290 °C, Capillary Voltage: −42 V, Tube lens Voltage: −137 V, Sheath Gas: 38, Sweep Gas: 0, Auxiliary Gas: 8. Overview spectra after 5 minutes and 2h reaction time are shown in **Supplementary Figures 4** and **Supplementary Figures 5**, respectively. Assignable high-resolution mass peaks are shown in **Supplementary Figure 6** and **Supplementary Figure 7**.

5.2 Mass spectra of the reaction solution

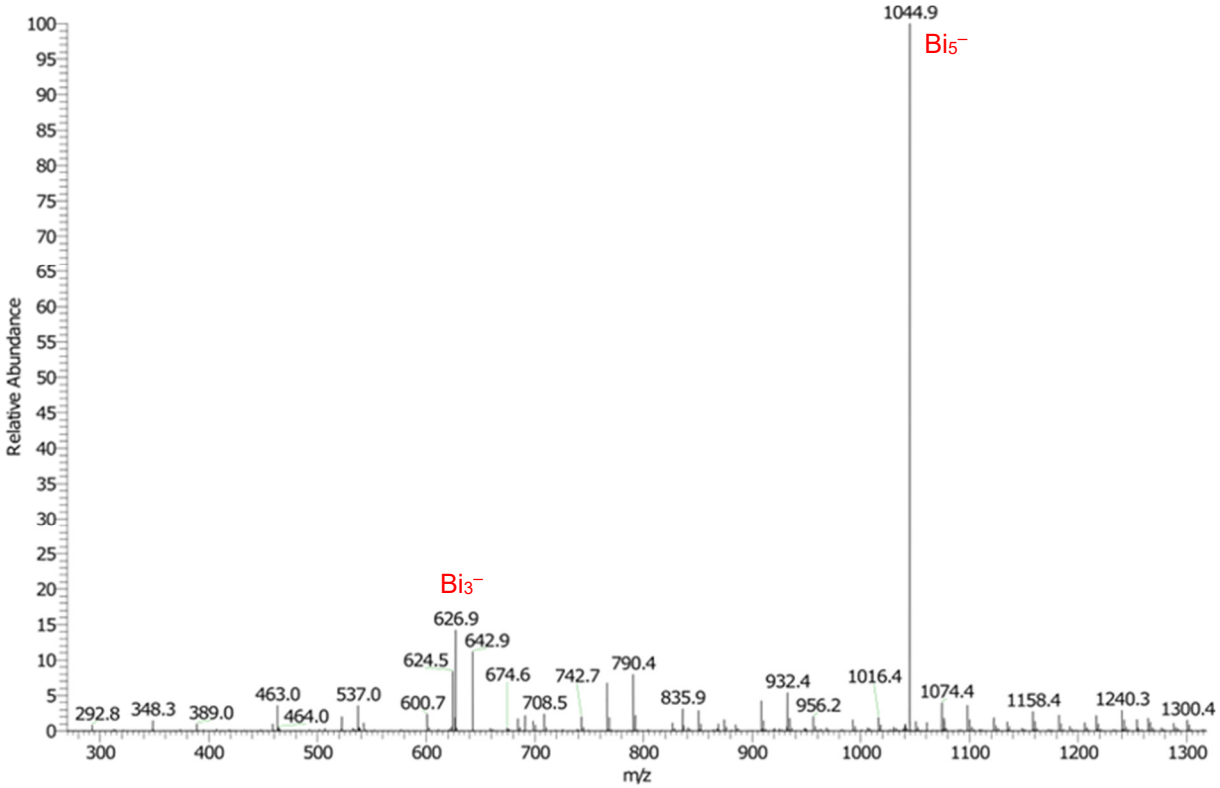

Supplementary Figure 4 | Overview ESI(−) mass spectrum recorded after 5 min reaction time. Identifiable mass peaks are indicated, which demonstrate the rapid and selective formation of Bi_5^- in the reaction mixture.

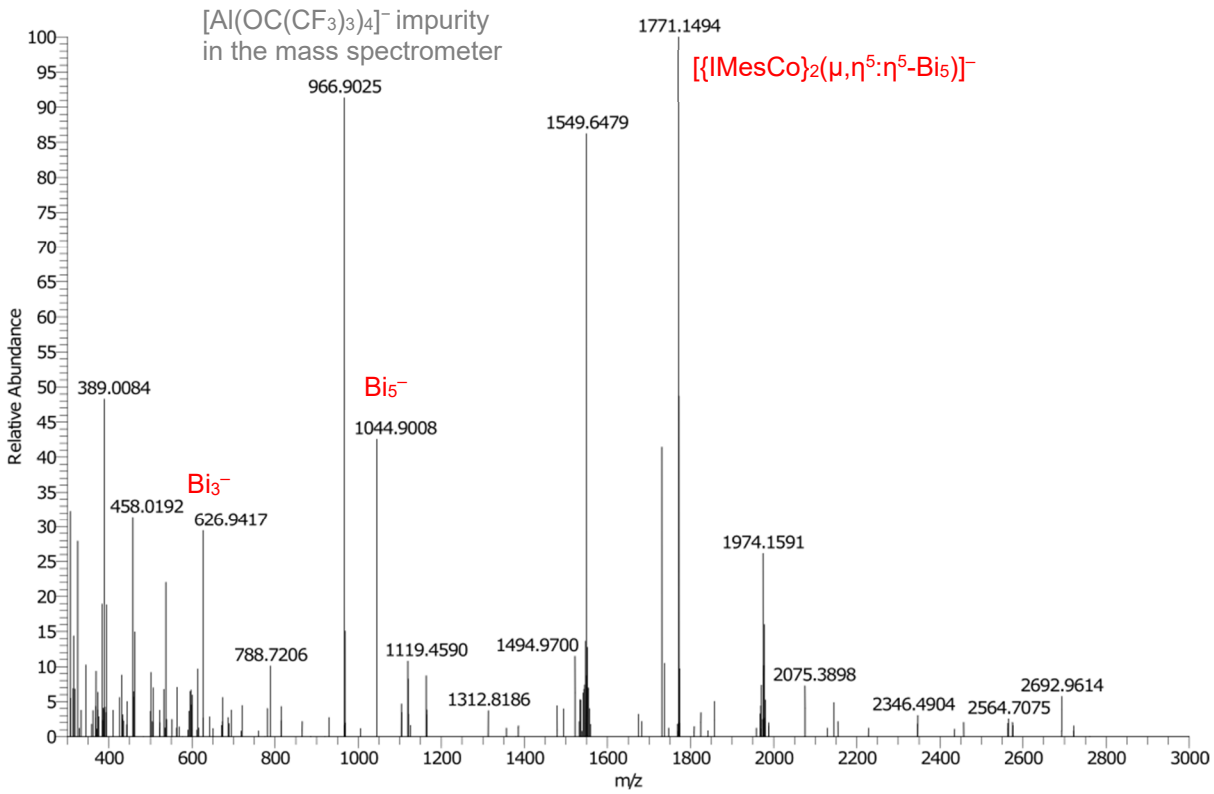

Supplementary Figure 4 | Overview ESI(−) mass spectrum recorded after 2 h reaction time. Most dominant identifiable mass peaks are indicated, with the predominant one demonstrating the abundance of complex **1** (in the form of its anion).

.

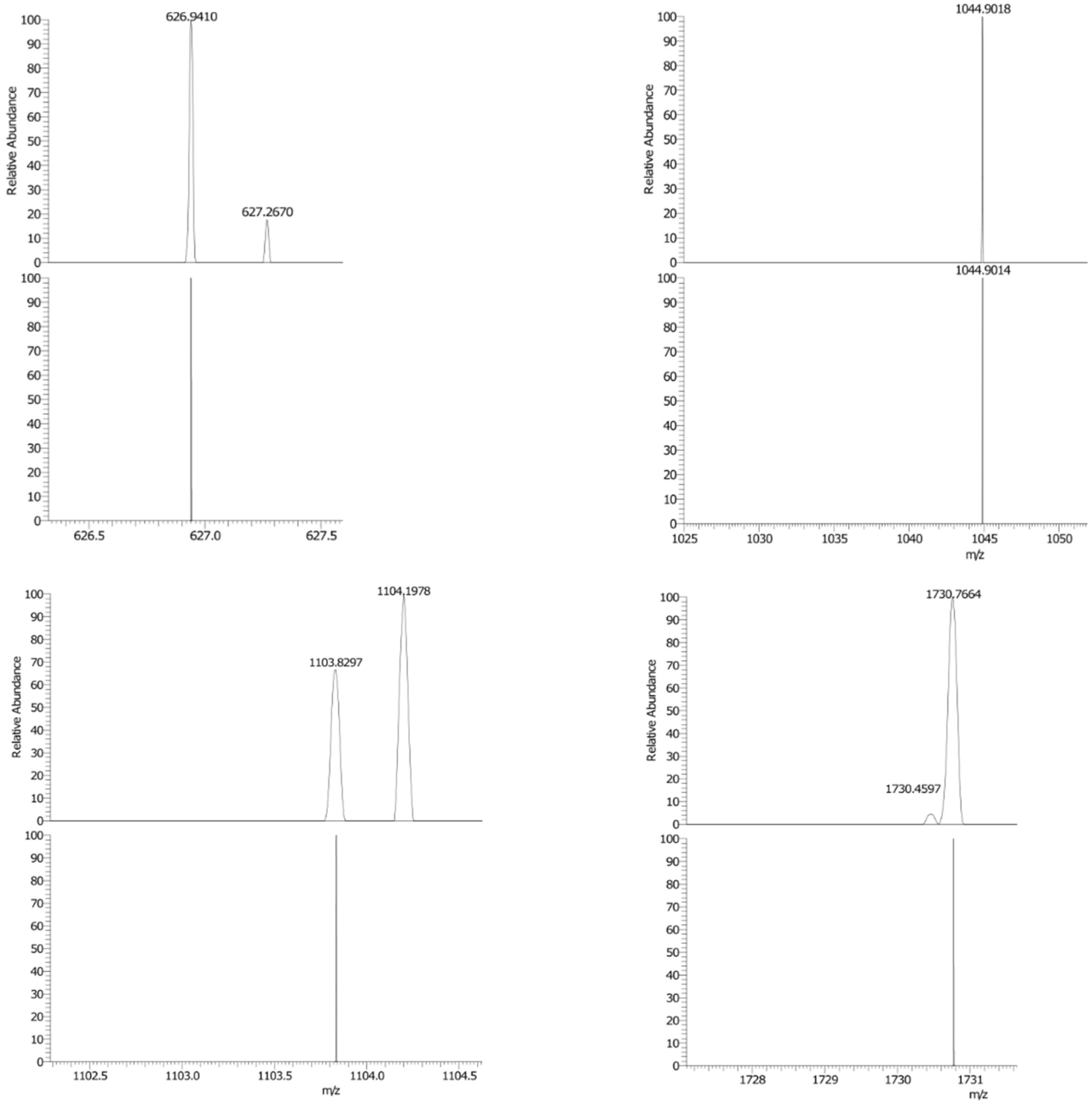

Supplementary Figure 5 | High-resolution ESI(–) mass spectra recorded after 2 h reaction time showing homometallic or heterometallic anions. The high-resolution spectra (upper curve: measured, below: simulated) indicate the existence of polybismuthide anions Bi_3^- (tope left) and Bi_5^- (tope right), as well as heterometallic fragments $(Bi_5Co)^-$ (bottom left) and $(Bi_8Co)^-$ (bottom right) of complex **1**.

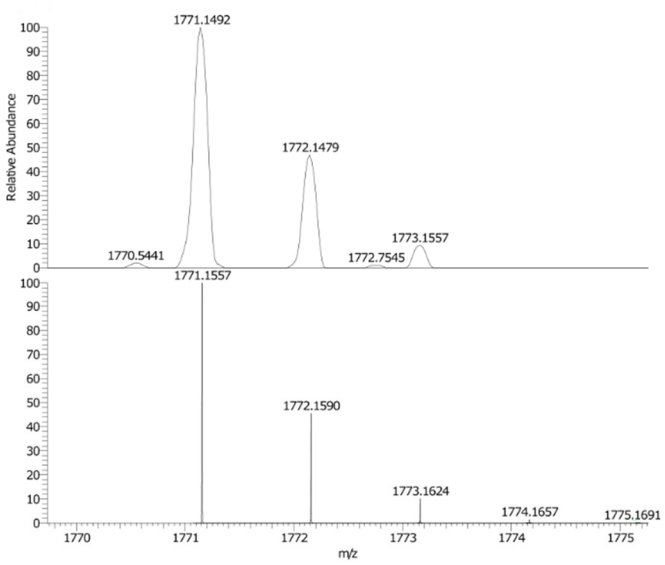

Supplementary Figure 6 | High-resolution ESI(–) mass spectrum in negative ion mode recorded after 2 h reaction time showing the anion of 1. The high-resolution spectrum refers to the existence of **1** in solution, detected as anion under ESI-MS conditions, prior to crystallization. Topmost: measured, below: simulated.

6 Magnetic studies: Derivative-field angle map from μ–SQUID *M*(*H*) loops

Employing the 3D vector magnet, *M*(*H*) loops at *T* = 30 mK were measured for different directions of applied field within the μ–SQUID plane. The derivatives d*M*/d*H* of the positive half-cycle are plotted with different in-plane angles as a d*M*/d*H* (H_x,H_y) color map, as shown in **Supplementary Figure 12**. Due to least magnetic coupling to the μ-SQUIDs, a certain direction (close to the *y* axis in this case) shows a white patch, i.e., the least magnitude of the derivative. Such a map is usually helpful to indicate the anisotropy in a system with large spin *J* (or *S*) and coupling (for example a dimer of 4f ions). However, here the anisotropy in the system is not clearly realized probably because of the isotropic *J* = *S* = 1/2 in this compound.

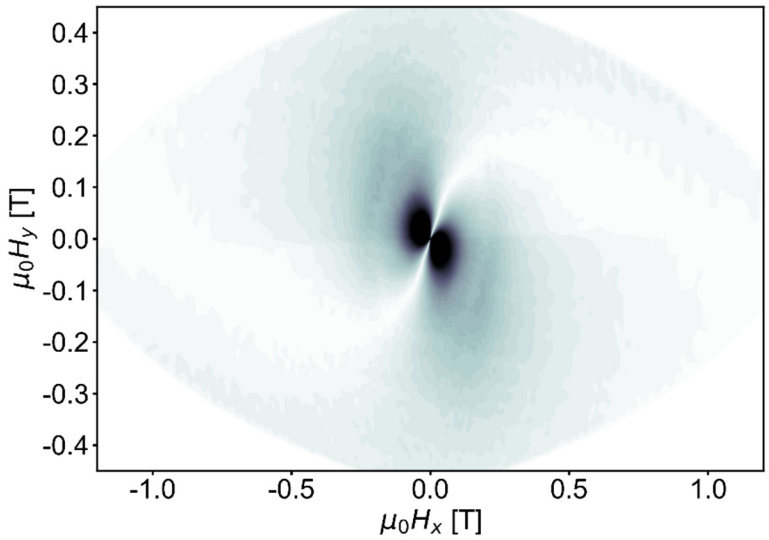

Supplementary Figure 12 | d*M*/d*H* (H_x,H_y) map obtained from positive half of the *M*(*H*) loops measured by a μ-SQUID at different in-plane angles.

7 Quantum Chemical Calculations

Quantum chemical calculations were done with TURBOMOLE.[3] An unbiased search of the global minimum of Bi_5^- was carried out with a genetic algorithm procedure.[4] In **Supplementary Table 3**, the Bi–Bi distance is listed for the most favourable structure, the planar ring (D_{5h}), as well as its energetic preference over the second stable isomer, a capped butterfly (C_{2v}), see **Figure 1b** in the main document, for several methods.

Supplementary Table 3 | Bi–Bi distance in the D_{5h} structure of Bi_5^- and energetic preference over the C_{2v} structure. The dhf-TZVP basis[5] together with Dirac-Hartree-Fock effective core potentials[6] was used unless explicitly mentioned otherwise.

Method	**d(Bi-Bi)/pm**	**ΔE/kJmol^{-1}**
PBE[7]	287.7	30
BP86[8,9]	287.9	39
TPSS[10]	286.6	21
PBE0[11]	283.5	20
B3LYP[12]	287.7	48
TPSSh[13]	285.0	18
HF[14]	282.9	19
MP2[15]	281.0	22
PBE, 2c-ECP[16], dhf-TZVP-2c basis[5]	291.3	66
PBE, scalar X2C,[17]x2c-TZVPall-2c basis[18]	286.7	32
PBE, 2c-X2C,[19] x2c-TZVPall-2c basis[18]	290.3	70

The electronic structure of the Bi_5^- ring is analogous to that of $(C_5H_5)^-$. The valence MOs of both species are shown in **Figure 1d** in the main document.

The title compound, [{IMesCo}$_2$Bi$_5$] (**1**) was additionally calculated with the hybrid functional PBE0. Images of MOs of the corresponding anion are shown in **Supplementary Figure 13** together with that obtained with PBE, structure parameters of the optimized structures of the anion and four electronic states of the neutral species as well as data concerning the electronic structure are listed in **Supplementary Table 4**. Most striking differences in the MOs is the high admixture of Bi contributions to the five highest occupied MOs in case of PBE0 and the shape of the HOMO. With PBE0 it is the binding MO between the Co atoms, which is HOMO-5 with PBE, whereas the two HOMOs with PBE are non-binding combinations of Co(d) orbitals.

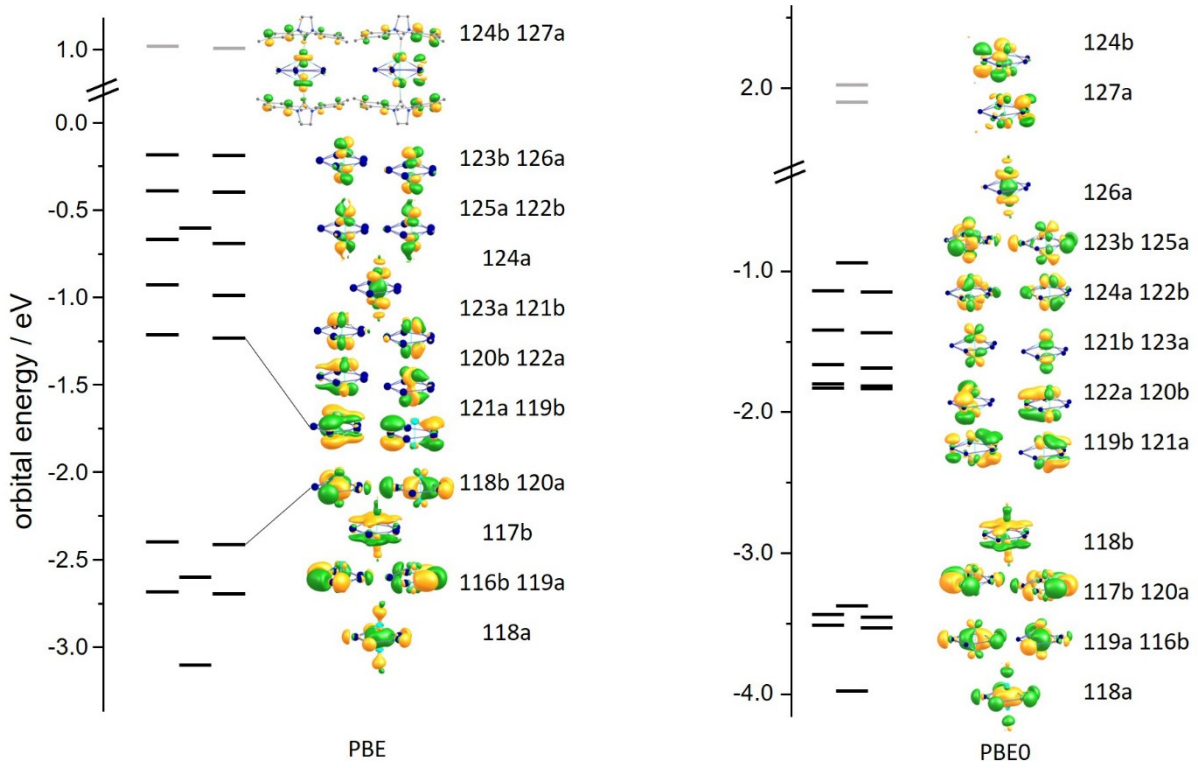

Supplementary Figure 13 | Valence MOs of [{IMesCo}$_2$Bi$_5$] (1) obtained with PBE and PBE0 functionals. The MOs calculated with PBE are shown to the left, those with PBE0 are shown to the right. Contours are drawn at 0.04 a.u.

Supplementary Table 4 | Geometric and electronic structure data of [{IMesCo}$_2$Bi$_5$] (1) and the hypothetical anion [{IMesCo}$_2$Bi$_5$]$^-$ obtained with the functional PBE0. Column labelling: Co–Co, Co–Bi and Bi–Bi are the (ranges of) distances between the corresponding atoms, C–Co–Co labels the bend of the Co–Co axis and the Co–C axes at the two Co atoms. *E* is the energy relative to the ^{2}A state in kJ/mol, in the following column, the S^2 values and their deviations from the value for the pure doublet/quartet are given, Gap denotes the HOMO-LUMO Gap and N_{ue} the number of unpaired electrons according to a Mulliken analysis[20] at the Co atoms and at the {Bi$_5$} ring. Row labelling: M$^-$ denotes the anionic (diamagnetic) species, the subsequent lines denote neutral species, in detail: In ^{2}A, the occupation of orbital 126a (HOMO within the irrep a) is reduced from 2 to 1, in ^{2}B that of 123b (HOMO within irrep b), ^{2}BS is a broken symmetry-state with overall one unpaired electron. In ^{4}A the unpaired electrons reside in 126a, 123b and 124b.

	Co–Co [Å]	C–Co–Co [°]	Co–Bi [Å]	Bi–Bi [Å]	*E* [kJ mol^{-1}]	S^2 (S^2-S[S+1])	Gap [eV]	N_{ue} (Co/Co/Bi5)
X-ray	2.52	176	2.75 – 2.79	2.90 – 2.91	–	–	–	–
Anion	2.48	177	2.68 – 2.78	2.87 – 2.88		0		0.0/0.0/0.0
^{2}A	2.60	170	2.67 – 2.90	2.89 – 2.92	0	1.423 (0.673)	2.691	0.77/0.77/–0.46
^{2}B	2.61	178	2.68 – 3.05	2.91 – 2.93	–30	1.541 (0.791)	1.803	1.08/1.08/–1.01
^{2}BS	2.97	179/169	2.78 – 3.19	2.92 – 2.95	–141	2.562 (1.812)	1.711	2.08/–1.94/0.86
^{4}A	3.12	170	2.79 – 3.25	2.92 – 2.93	–143	4.563 (0.813)	2.030	2.02/2.02/–0.98

Whereas for the anion PBE0 structure parameters agree reasonably well with PBE and also with the experimental data for the neutral species, unphysically large deviations in the Co–Co distance and in the Co–Bi distances are observed for the neutral species, i.e., as soon as one of the HOMOs of the anion is depleted. This is particularly true for the energetically seemingly favourable states ^{2}BS and ^{4}A, for which the Co–Co distance is calculated 45 pm and 60 pm too long. This comes along with high spin contaminations. Apparently PBE0 and (probably) all other hybrid functionals as well as calculations basing on Hartree-Fock wave functions fail in the description of this compound.

Supplementary Figure 14 shows the MOs of structures related to [{IMesCo}$_2$Bi$_5$] (**1**), namely [{IMesNi}$_2$P$_5$][21] and [{(C$_5$H$_5$)Mo}$_2$As$_5$],[22] in relation to those of the former, in all cases for the anionic closed-shell structures. Albeit the mixing between orbitals of the five-membered ring and the transition metal differs for the three compounds, the identification of related MOs is still possible and indicated with connecting lines in **Supplementary Figure 15**. The Ni compound has two more valence electrons than the Co compound, thus the LUMO of the latter becomes the HOMO of the former, LU(Co)→HO(Ni). The Mo compound has six valence electrons less than the Co compound, which leads to the following consequences. The analogues of HO(Co) and HO–1(Co), which are located exclusively at the transition metal atoms, are no longer occupied. HO–2(Co) and HO–3(Co), which are dominated by d(Co) with (small) admixtures from the neighbouring C atoms of the IMes groups significantly change their character in the Mo compound: HO–12(Mo) and HO–13(Mo) also show contributions from the d orbitals and from the ligand, but here dominated by the latter ((C$_5$H$_5$)$^-$). Further, HO–5(Co) and HO–6(Co) become HO(Mo) and HO–1(Mo), while HO–4(Co) becomes HO–2(Mo).

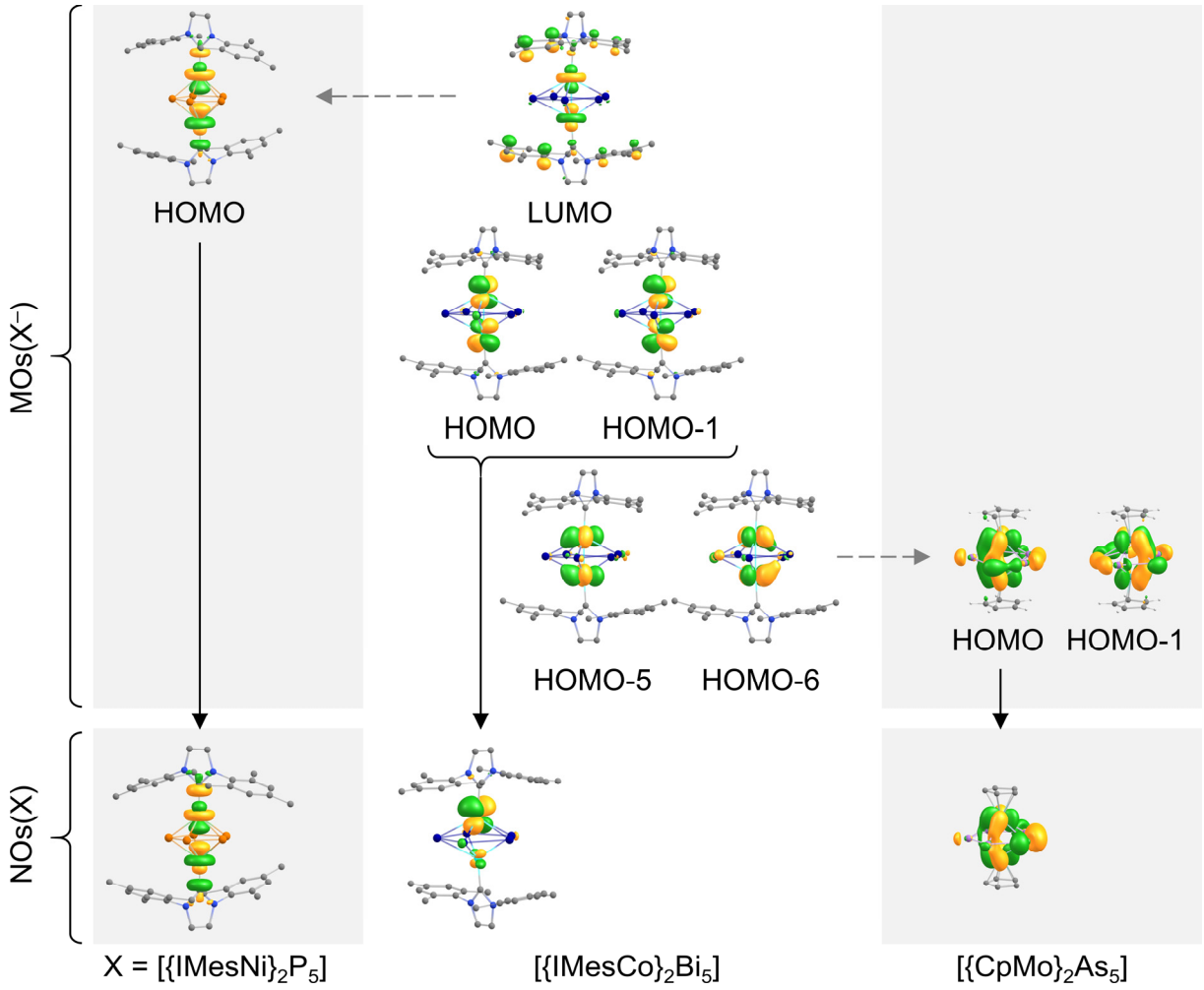

Supplementary Figure 14 | Comparison of frontier orbitals and natural orbitals of calculated species $[\{IMesNi\}_2P_5]^-$ $[\{IMesCo\}_2Bi_5]^-$, and $[\{(C_5H_5)Mo\}_2As_5]^-$. Upper part: Frontier molecular orbitals (MOs) of $[\{IMesCo\}_2Bi_5]^-$, $[\{IMesNi\}_2P_5]^-$ and $[\{(C_5H_5)Mo\}_2As_5]^-$ (similar situation as for $[\{(1,2,4\text{-}t\text{Bu}_3C_5H_2)Mo\}_2Sb_5]^-$, which is not shown here) in their optimized structures. Lower part: Natural orbitals (NOs) with occupation eigenvalue close to one for their neutral counter parts (doublet states) in the X-ray structure.

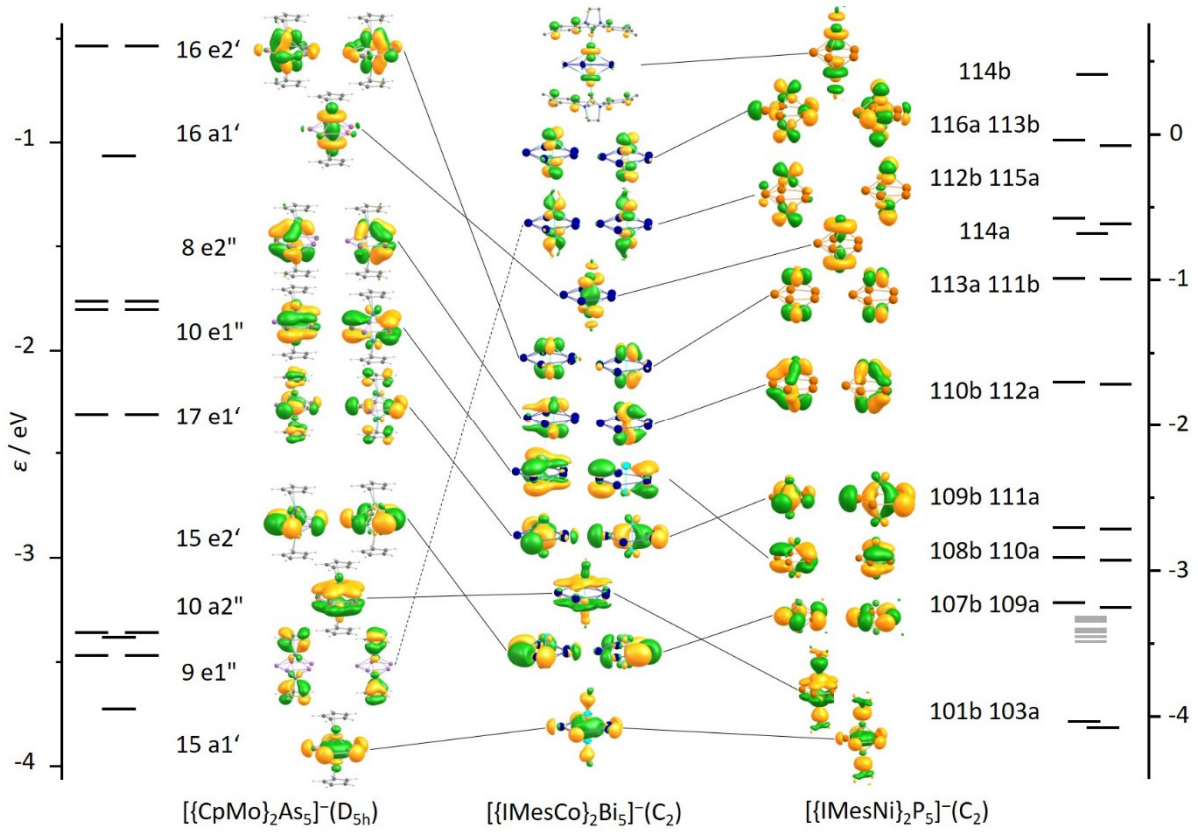

Supplementary Figure 15 | Images of occupied valence orbitals of structures related to hypothetic anion [{IMesCo}$_2$Bi$_5$]$^-$. The results for [{IMesCo}$_2$Bi$_5$]$^-$ are shown in the middle, between those of related compounds, namely hypothetical anion [{(C$_5$H$_5$)Mo}$_2$As$_5$]$^-$ (left; similar situation as for [{(1,2,4-*t*Bu$_3$C$_5$H$_2$)Mo}$_2$Sb$_5$]$^-$, which is not shown here) and hypothetical anion [{IMesNi}$_2$P$_5$]$^-$ (right); for [{IMesCo}$_2$Bi$_5$]$^-$ additionally the LUMO is shown (middle, top), for [{IMesNi}$_2$P$_5$]$^-$ a bundle of MOs between -3 and -4 eV with contributions solely from the IMEs groups is listed only in the energy level diagram (gray bars). IMes groups are omitted for clarity, except for the LUMO of the Co compound, which is the only orbitals shows significant contributions from this groups.

8 References

1. Sheldrick, G. M. SHELXT-integrated space-group and crystal-structure determination. *Acta Crystallogr. A Struct. Chem.* **71**, 3–8 (2015).
2. K. Brandenburg, Diamond, Crystal Impact GbR, Bonn, Germany, 2021
3. TURBOMOLE pre-version 7.7 2022 (University of Karlsruhe and Forschungszentrum Karlsruhe, 1989–2007, and TURBOMOLE, since 2007, accessed 13 February 2022); http://www.turbomole.com.
4. Sierka, M. *et al.* Unexpected structures of aluminum oxide clusters in the gas phase. *Angew. Chem. Int. Ed.* **46**, 3372–3375 (2007).
5. Weigend, F. & Baldes, A. Segmented contracted basis sets for one- and two-component Dirac-Fock effective core potentials. *J. Chem. Phys.* **133**, 174102 (2010).
6. Metz, B., Stoll, H. & Dolg, M. Small-core multiconfiguration-Dirac-Hartree-Fock-adjusted pseudopotentials for post-d main group elements: Application to PbH and PbO. *J. Chem. Phys.* **113**, 2563–2569 (2000).
7. Perdew, J. P., Burke, K. & Ernzerhof, M. Generalized Gradient Approximation Made Simple. *Phys. Rev. Lett.* **77**, 3865–3868 (1996).
8. Perdew, J. P. Density-functional approximatino for the correlation energy of the inhomogeneous electron gas. *Phys. Rev. B.* **33**, 8822–8824 (1986).
9. Becke, A. D. Density-functional exchange-energy approximation with correct asymptotic behaviour. *Phys. Rev. A.* **38**, 3098–3100 (1988).
10. Tao, J., Perdew, J. P., Staroverov, V. N. & Scuseria, G. E. Climbing the density functional ladder: Nonempirical meta–generalized gradient approximation designed for molecules and solids. *Phys. Rev. Lett.* **91**, 146401 (2003).
11. Perdew, J. P. & Ernzerhof, M. Rationale for mixing exact exchange with density functional approximations. *J. Chem. Phys.* **105**, 9982–9985 (1996).
12. Lee, C., Yang, W. & Parr, R. G. Development of the Colic-Salvetti correlation-energy formula into a functional of the electron density. *Phys. Rev. B.* **37**, 785–789 (1988).
13. Staroverov, V. N., Scuseria, G. E., Tao, J. & Perdew, J. P. Comparative assessment of a new nonempirical density functional: Molecules and hydrogen-bonded complexes. *J. Chem. Phys.* **119**, 12129–12137 (2003).
14. Häser, M. & Ahlrichs, R. Improvements on the direct SCF method. *J. Comput. Chem.* **10**, 104–111 (1989).
15. Weigend, F. & Häser, M. RI-MP2: First derivatives and global consistency. *Theor. Chem. Acc.* **97**, 331–340 (1997).

16. Baldes, A. & Weigend, F. Efficient two-component self-consistent field procedures and gradients: Implementation in Turbomole and application to Au-20. *Mol. Phys.* **111**, 2617–2624 (2013).
17. Peng, D., Middendorf, N., Weigend, F. & Reiher, M. An efficient implementation of two-component relativistic exact-decoupling methods for large molecules. *J. Chem. Phys.* **138**, 184105 (2013).
18. Pollak, P. & Weigend, F. Segmented Contracted Error-Consistent Basis Sets of Double- and Triple-ζ Valence Quality for One- and Two-Component Relativistic All-Electron Calculations. *J. Chem. Theory Comput.* **13**, 3696–3705 (2017).
19. Franzke, Y. J., Middendorf, N. & Weigend, F. Efficient implementation of one- and two-component analytical energy gradients in exact two-component theory. *J. Chem. Phys.* **148**, 104110 (2018).
20. R. S. Mulliken. Electronic Population Analysis on LCAO-MO Molecular Wave Functions. *J. Chem. Phys* **23**, 1833–1840 (1955).
21. Hierlmeier, G., Coburger, P., van Leest, N. P., de Bruin, B. & Wolf, R. Aggregation and Degradation of White Phosphorus Mediated by N-Heterocyclic Carbene Nickel(0) Complexes. *Angew. Chem. Int. Ed.* **59**, 14148–14153 (2020).
22. Rheingold, A. L., Foley, M. J. & Sullivan, P. J. "Triple-Decker Sandwich" with a Planar As5 Ring. Synthesis and Crystal Structure of CpMo[μ-(η^4-As$_5$)]MoCp. *J. Am Chem. Soc.* **104**, 4727–4729 (1982).